Experimental study of the band structure of GaP, GaAs, GaSb, InP, InAs, and InSb

Gwyn P. Williams
National Synchrotron Light Source, Brookhaven National Laboratory, Upton, New York 11973

F. Cerrina
Department of Electrical and Computer Engineering, University of Wisconsin—Madison, Madison, Wisconsin 53706

G. J. Lapeyre, J. R. Anderson, R. J. Smith, and J. Hermanson
Physics Department, Montana State University, Bozeman, Montana 59717

(Received 23 September 1985)

An experimental study of the band structures of GaP, GaAs, GaSb, InP, InAs, and InSb has been made with use of polarization-dependent angle-resolved photoemission. We describe an analysis of the data which allowed us to do band mapping (E vs $\mathbf{k}_\perp$) among some 30 bands both occupied and unoccupied, distributed in the range from 20 eV above to 8 eV below the valence-band maximum. The measurements were made for the $\langle 110 \rangle$ direction Γ—K—X along line Σ in the Brillouin zone. The experiments utilized synchrotron-radiation-induced photoemission in which the polarization of the light and collection angles of the electrons were carefully controlled. We compare the data with calculated band structures and tabulate critical-point energies.

I. INTRODUCTION

We have made an extensive experimental study of the band structures of the six III-V semiconductor compounds GaP, GaAs, GaSb, InP, InAs, and InSb with use of polarization-dependent angle-resolved photoemission in the range $10 < \hbar\omega < 30$ eV. The studies were made along the $\langle 110 \rangle$ crystallographic direction, normal to the [110] cleavage plane. This corresponds in reciprocal-lattice space to investigations from the zone center at Γ to point K then to point X, along the Σ line.

There have been many calculations to date of the intrinsic band structures[1,2] of the III-V compound semiconductors and several experimental determinations of the GaAs and GaP bands.[3–5] An excellent review has been presented by Ley and Cardona.[6] The most comprehensive studies have been concerned primarily with the occupied bands 1—4. Conduction bands have been studied but with few data points. We have previously reported some of the preliminary findings of this work on InAs.[7]

In this paper we report studies which we have made for both occupied and unoccupied bands for all six of the III-IV compounds mentioned previously. We also include detailed discussions of the methods used to extract the wave-vector information from the experimental data and hence do "band mapping." Briefly the method involves a correlation of the experimental results with the predictions of a theoretical band-structure calculation to determine values of $k_\perp$, the normal component of momentum for the interband transitions observed in the spectra. The theoretical bands are then adjusted as needed to improve the agreement with the data. Taking into account symmetry selection rules and the possibility of surface umklapp processes, we were able to account for almost all the peaks in the experimental spectra in terms of the initial and final bands. We were then able to reconstruct the

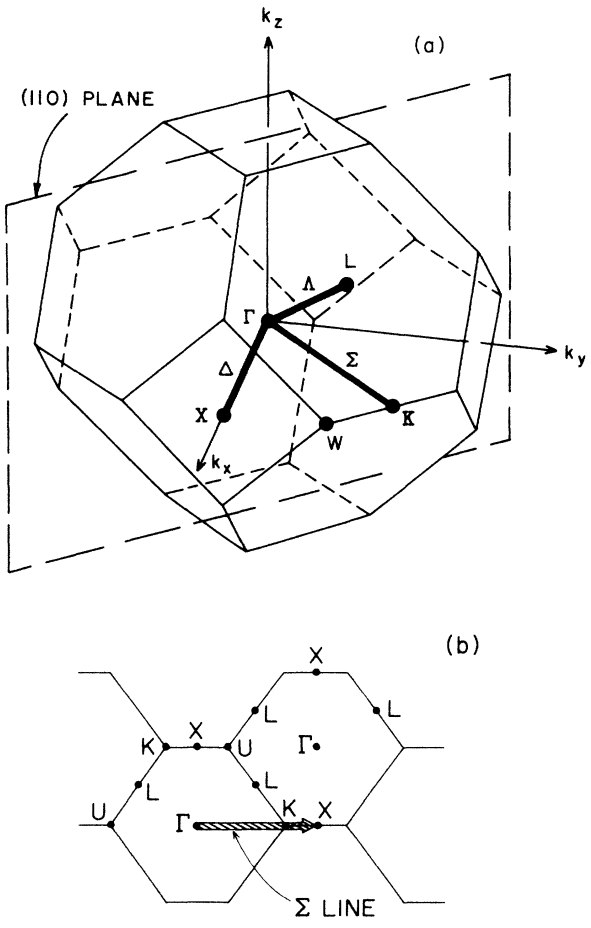

FIG. 1. (a) Face-centered-cubic Brillouin zone showing the (110) cleavage plane. (b) Cross section through an extended fcc Brillouin-zone scheme showing the Σ line.

band structure of the materials in the region of the Brillouin zone investigated. Our data cover some 30 bands lying in energy from 8 eV below the valence-band maximum (VBM) to 20 eV above it.

II. III-V COMPOUND LATTICE STRUCTURE AND PHOTOEMISSION GEOMETRY

The III-V compounds have the face-centered-cubic structure, the Brillouin zone for which is shown in Fig. 1(a). The crystals cleave readily to reveal the [110] surface whose plane is shown in the figure. We also show in Fig. 1(b) a cross section through an extended Brillouin zone scheme perpendicular to the [110] surface. The [110] surface in real space is depicted in Fig. 2, which shows the single mirror plane (MP) and the Ga empty dangling bond direction. We label this the $\phi=0°$ azimuth, and increase azimuthal angles in a clockwise direction when looking at the crystal face from above.

Due to the high density of bands the photoemission spectra from the III-V compounds contain a large number of peaks. To prevent overlapping of peaks it was necessary to carefully control the number of allowable transitions in a given spectrum.

The first restriction we imposed was geometrical and was to confine all our studies to normal emission $\pm 2°$. Thus, both electron energy and momentum were determined experimentally. For normal emission the electron momentum parallel to the surface both inside and outside the crystal is zero. The only allowable transitions we could observe then were those along the Σ line which runs from Γ to point K then point X and is shown in Fig. 1. Thus, the volume of $\mathbf{k}$ space from which transitions could be detected was limited.

The second restriction we made was to control the orientation of the electric vector $\mathbf{A}$ of the incident light. Polarized light of these wavelengths (300—2000 Å) was obtained from the Tantalus 1 240-MeV electron storage ring at the University of Wisconsin-Madison.

Synchrotron radiation from the storage ring was passed through a 1-m normal-incidence Rowland circle monochromator with a resolving power of 200. A refocusing mirror produced a demagnified image of the monochromator exit slit on the sample which was located at the focus point of a double-pass cylindrical mirror analyzer (CMA). The CMA was usually operated at a pass energy of 15 eV, giving a combined resolving power for the electron spectrometer and monochromator of about 300 MeV. The useful photon energy range was from 5 to 30 eV. The samples were cleaved *in situ* using a sharpened tungsten carbide blade against a copper anvil. The crystal fracture was produced by a slow increase in force of the blade against the anvil.

The incident light geometries we used were (1) normal incidence, $\mathbf{A}$ parallel to the MP, (2) normal incidence, $\mathbf{A}$ perpendicular to the MP, (3)—(5) p polarization, oblique incidence at azimuthal angles of 180°, 0°, and 90°, respectively. Note that $\mathbf{A}$ is approximately parallel or perpendicular, respectively, to the empty dangling bond in geometry (4) or (3).

In order to achieve geometries of this kind, the CMA itself was modified[8] to allow the light beam to pass through the CMA cylinders at the magic angle of 42.3° from the CMA axis. A further modification to the CMA was the addition of a drum and aperture, as shown in Fig. 3, which passes a restricted azimuthal portion ($\pm 2°$) of the cone of trajectories passed by a conventional CMA. The drum rotates about the CMA axis permitting the azimuthal collection angle to be varied freely. If the sample normal is along the CMA axis (C), an azimuthal scan of emission angles can be made for the fixed polar angle of 42.3°. In addition, a special manipulator was constructed which placed the sample normal along the CMA acceptance cone direction. The sample could be rotated independently about its own normal and about the CMA axis.

Relating this special equipment to the experiment, the required geometries were achieved as follows. For normal incidence the sample was situated as shown in Fig. 3. Thus, no matter how impure the polarization of the source, the $\mathbf{A}$ vector was parallel to the sample surface. We estimate the polarization purity to be 88% at 20 eV.

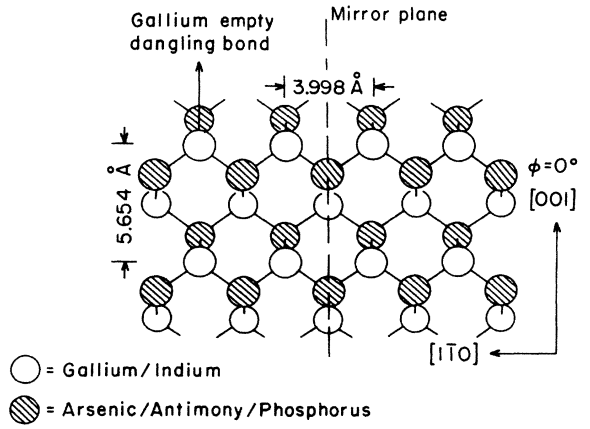

FIG. 2. Schematic of the GaAs(110) surface showing the mirror plane and the direction of the Ga empty dangling bond which defines azimuth $\Phi=0°$.

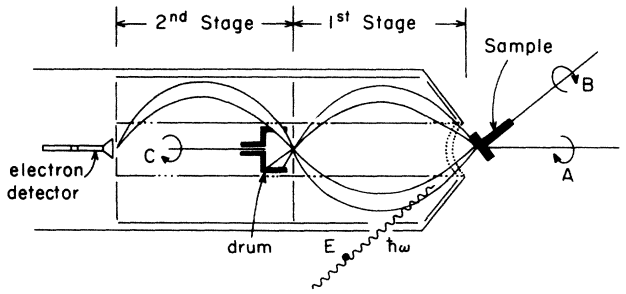

FIG. 3. Schematic of the experimental geometry showing the cylindrical-mirror electron-energy analyzer modified by adding an angle-resolved drum capable of rotation about an axis C. Also indicated is the modification to allow the incoming light to enter through the cylinder walls at an angle of 42.3° with the main cylinder axis. The sample manipulator allowed rotations about either axis A or B. The electric vector of the incident light was normal to the figure.

For this normal-incidence geometry, the sample was then rotated about its normal to place the major component of the A vector along the desired azimuth. For the oblique incidence cases, we rotated the sample normal by 90° around the CMA axis and lined up the drum to accept again only the normally emitted electrons. The sample was then rotated about its own normal to orient the MP with respect to the radiation vector. Since the radiation was not 100% polarized, there was a significant but small component of s polarization present in these orientations.

Lapeyre *et al.*[9] have described the ways in which the continuum of synchrotron radiation can be used to study the emission surface, $N(E_f,\hbar\omega)$, for a given material. Scans of photon energy at fixed analyzer kinetic energy (constant final energy spectroscopy or CFS), and with synchronously scanned kinetic energy (constant initial energy spectroscopy or CIS), when combined with the more traditional scan of analyzer kinetic energy at fixed photon energy (energy distribution curve or EDC), were all used as needed to help locate critical points or other points of special interest in the band structure of these compounds. Only a few of the literally hundreds of EDC's collected in this investigation are presented here.

III. RESULTS AND ANALYSIS

A. Method of analyzing data

We show in Figs. 4–7 angle-resolved energy distribution curves for selected polarizations for InAs, InSb, InP, and GaSb. The main problem in analyzing the data and extracting band-structure information from the set of experimentally obtained spectra stems from the fact that there is nothing explicit in the experimental spectra that identifies the initial or final band or, assuming direct transitions, the value of $\mathbf{k}_\perp$ involved in an observed transition. In fact, the information that can be obtained from the experimental data independent of specific assumptions include the initial- and final-state energies [relative, say, to the valence-band maximum (VBM)] of the transitions observed as peaks in the spectra, and the value of $k_\parallel$, which is $k_\parallel=0$ in the present case of normal emission.

This amount of information is insufficient for our goal, which is to infer as much as possible about the energy bands (along the Σ line) from the experimental spectra. Additional information and assumptions are needed, and these are introduced in the following way. From existing band-structure calculations we take a set of calculated bands for comparison with the experimental data, with the assumption that the theoretical bands are reasonably realistic in terms of their general shape, the ordering of the bands and the energies of the critical points. We also assume that the peaks observed in the experimental spectra represent interband transitions with a characteristic value of $\mathbf{k}_\perp$ which is conserved.

In practice, the method of analyzing the data in the framework of the assumed theoretical bands amounts to the following. For a given material and a given experimental geometry we display graphically the data contained in a collection of spectra as a structure plot. This is a plot of the initial-state energy, on the vertical axis, versus the photon energy, on the horizontal axis of all of the features (peaks, shoulders, etc.) in the spectra. By referring to Fig. 8 we can illustrate how this is done. If the band structure of a hypothetical material is as in Fig. 8(a), then at a photon energy $\hbar\omega=14$ eV there will be a direct transition at A, and this transition will be observed

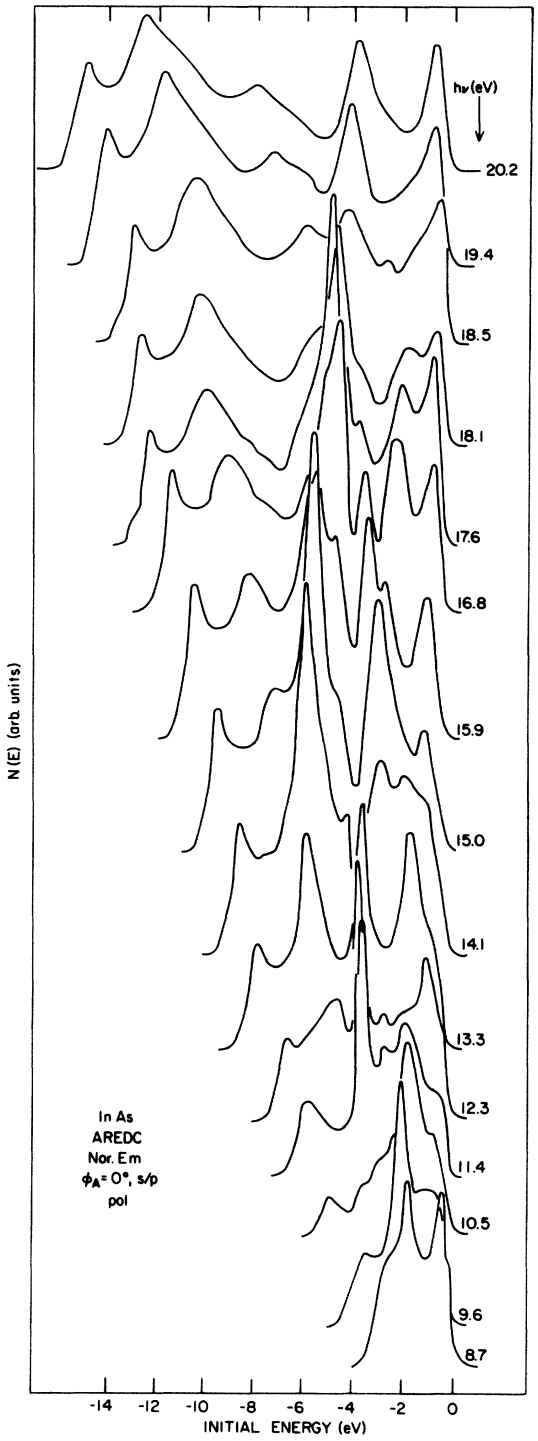

FIG. 4. Photoemitted angle-resolved energy distribution curves obtained from an InAs(110) surface with light at oblique incidence at an azimuthal angle of 0°.

as the peak A in Fig. 8(c). The initial-state energy E_i and photon energy $\hbar\omega$ are known experimental parameters, and they are plotted in Fig. 8(b) as the point A.

A theoretical structure plot is then constructed using the theoretical bands for the material. This construction is identical in principal to that of the experimental structure plot: One infers, with due allowance for selection rules, the number and arrangement of the peaks in the spectra that would be obtained in a hypothetical experiment. The value of E_i and of $\hbar\omega$, the energy difference between initial and final bands, can be read off directly from the band-structure diagram. The complete theoretical structure plot will consist of a set of lines, one for each valence-band—conduction-band pair.

The solid line passing through A in Fig. 8(b) is the theoretical structure plot for the bands in Fig. 8(c). It is easy to see that, by construction, $\mathbf{k}_\perp$ is a unique running parameter out along the theoretical structure plot, and a number of such values are accordingly noted. Given the

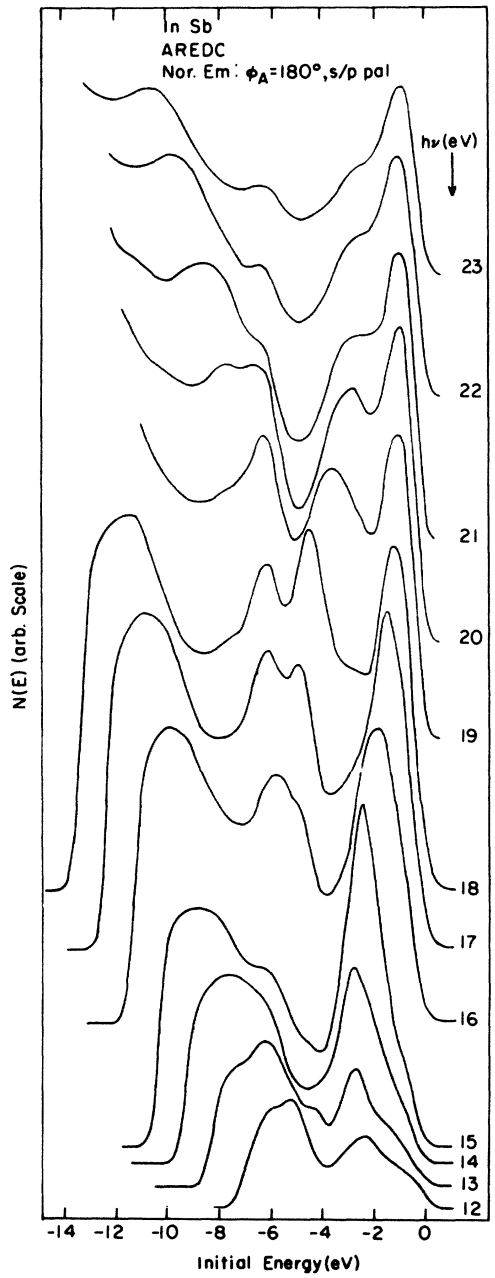

FIG. 5. Photoemitted angle-resolved energy distribution curves obtained from an InSb(110) surface with light at oblique incidence at an azimuthal angle of 180°.

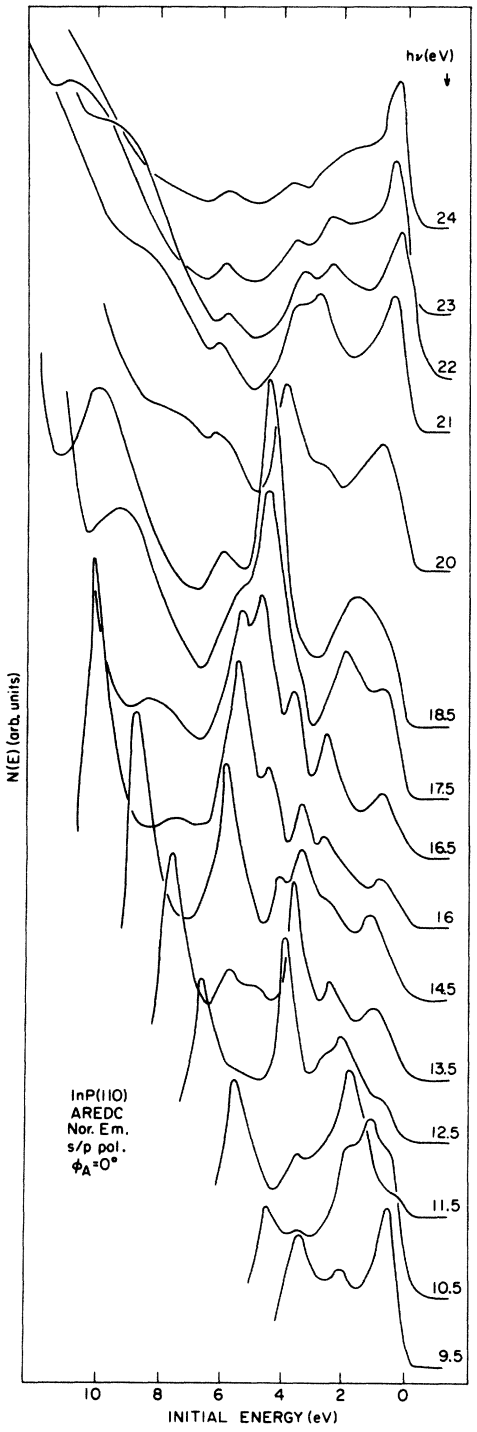

FIG. 6. Photoemitted angle-resolved energy distribution curves obtained from an InP(110) surface with light at oblique incidence at an azimuthal angle of 0°.

various assumptions in this treatment, the $\mathbf{k}_\perp$ value corresponding to peak A can then be read off the theoretical structure plot.

If the theoretical bands accurately represent the experimental situation, and if the assumptions used in this treatment are valid, then the experimental and theoretical structure plots should coincide, as in the synthetic example of Fig. 8, and one can identify the $\mathbf{k}_\perp$ value for each peak. In practice, the correspondence is far from perfect. Nonetheless, justification of the method used and corroboration of the validity of the assumptions made stems from the following circumstance: The shapes and mutual arrangement of the energy bands result in a characteristic pattern in the theoretical structure plot. For all the materials studied, while a point-by-point comparison of the experimental and theoretical structure plots do show deviations, nonetheless the characteristic pattern is replicated by the experimental data to such a degree and with so many points of correspondence as can only be reasonably explained by the essential joint correctness of the assumed band structure, the procedure, and the inherent assumptions.

The III-V semiconductor compounds we studied have very similar band structures, and we carry through this analysis in detail here only for GaAs. The trial band structure we used for this material consists of the three

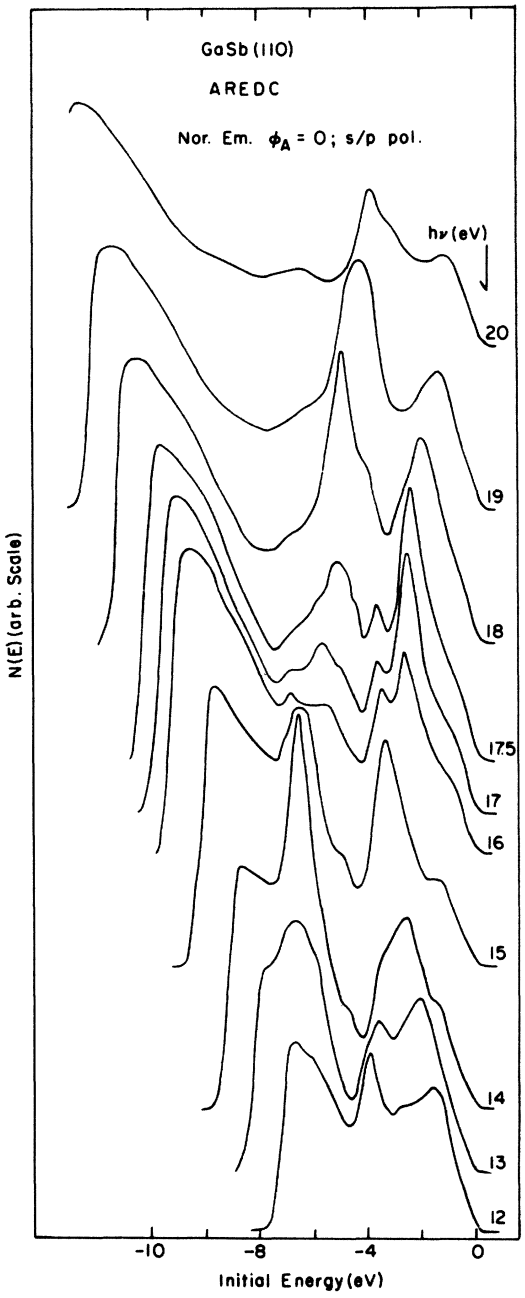

FIG. 7. Photoemitted angle-resolved energy distribution curves obtained from a GaSb(110) surface with light at oblique incidence at an azimuthal angle of 0°.

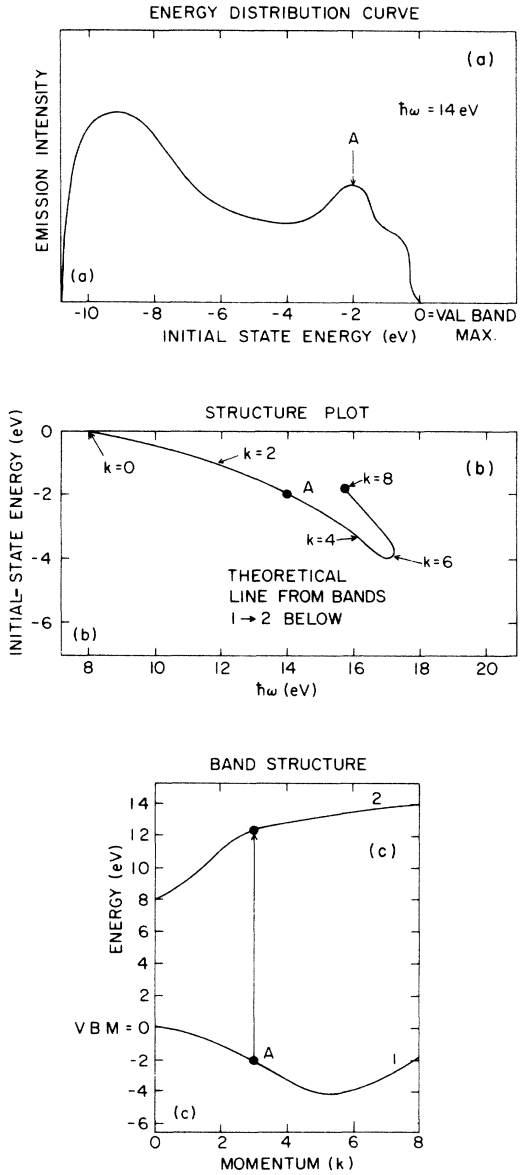

FIG. 8. Illustration of the technique for band mapping (a) fictitious energy distribution curve; (b) structure plot showing the peak from (a) as a closed circle and the theoretical line derived from the bands depicted in (c); and (c) the data as it would appear plotted on the band-structure diagram.

TABLE I. Theoretical structure plots for initial band 2 to final band 6 for GaAs, GaP, GaSb, InAs, InP, and InSb in the ⟨110⟩ direction from $\Gamma(k=0)$ to $X(k=20)$. Data in this form for all pairs of initial (i) to final (f) bands is available from the Physics Auxiliary Publication Service (Ref. 11).

Band			GaAs		GaP		GaSb		InAs		InP		InSb	
1	f	k	E_i	$\hbar\omega$	E_i	$\hbar\omega$	E_i	$\hbar\omega$	E_i	$\hbar\omega$	E_i	$\hbar\omega$	E_i	$\hbar\omega$
2	6	0	0.4	5.0	0.1	5.3	0.8	5.1	0.5	5.0	0.4	4.9	0.3	4.3
2	6	1	0.5	5.1	0.4	5.5	1.0	5.2	0.7	5.1	0.6	5.1	0.7	4.7
2	6	2	1.1	5.7	0.7	5.8	1.2	5.4	1.1	5.5	1.0	5.5	1.3	5.2
2	6	3	1.7	6.3	1.4	6.5	1.8	5.9	1.7	6.0	1.5	5.9	1.8	5.7
2	6	4	2.5	7.2	2.1	7.2	2.3	6.4	2.3	6.6	2.2	6.6	2.7	6.5
2	6	5	3.2	8.1	2.6	7.8	2.9	7.0	3.0	7.3	2.8	7.3	3.4	7.3
2	6	6	3.7	8.8	3.2	8.5	3.4	7.6	3.5	7.9	3.5	8.0	3.8	7.7
2	6	7	4.3	9.7	3.9	9.4	4.1	8.4	4.1	8.7	4.0	8.7	4.3	8.4
2	6	8	4.9	10.6	4.4	10.2	4.6	9.2	4.8	9.6	4.4	9.4	4.7	8.9
2	6	9	5.3	11.4	4.9	11.0	5.0	9.9	5.1	10.1	4.9	10.2	5.1	9.6
2	6	10	5.7	12.3	5.3	11.7	5.3	10.5	5.5	10.8	5.1	10.8	5.4	10.1
2	6	11	6.0	12.9	5.8	12.6	5.7	11.3	5.8	11.4	5.4	11.4	5.7	10.8
2	6	12	6.2	13.4	6.1	13.3	5.9	11.8	6.0	12.0	5.6	12.0	6.0	11.4
2	6	13	6.4	13.7	6.4	13.6	6.1	12.2	6.2	12.4	5.8	12.4	6.3	11.8
2	6	14	6.6	13.1	6.6	13.2	6.3	11.9	6.3	12.0	6.0	12.0	6.4	11.5
2	6	15	6.7	12.2	6.8	12.5	6.5	11.3	6.4	11.3	6.1	11.2	6.5	10.8
2	6	16	6.8	11.4	6.9	11.6	6.6	10.6	6.5	10.6	6.2	10.5	6.5	10.2
2	6	17	6.8	10.5	7.0	10.8	6.7	10.0	6.5	10.0	6.2	9.7	6.6	9.7
2	6	18	6.9	9.9	7.1	10.1	6.7	9.5	6.6	9.5	6.2	9.2	6.7	9.3
2	6	19	6.9	9.5	7.1	9.7	6.8	9.2	6.7	9.3	6.2	8.8	6.7	9.0
2	6	20	6.9	9.3	7.1	9.6	6.8	9.1	6.6	9.1	6.2	8.7	6.6	8.9

valence bands, from the calculations of Chelikowski and Cohen,[1] and a number of conduction bands, taken from Pandey's calculations[2] based on the pseudopotentials of Cohen and Bergstresser.[10]

We have tabulated the theoretical structure plots derived from the band structure we used for all the materials studied[11] and as an example show the data for band 2 to band 6, as Table I.

B. Application to GaAs

From the theoretical bands for GaAs shown in Fig. 17 (which also contain the experimental points), we derived the theoretical structure plots involving initial band 2 (Fig. 9), initial band 3 (Fig. 10), and initial band 4 (Fig. 11). These structure plots also contain the experimental structure plot points appropriate to the particular initial band. The latter determination was made by assigning the experimental point to the closest structure plot line. In some cases, because of the local density of structure plot lines, a point lies an equal distance from two, and sometimes three lines. In such a case, when no distinction can be made, no distinction is made, and a single experimental point is assigned to two or more lines on the grounds of consistence within the model being used: Such a peak must be composite.

Consider, for example, in Fig. 9, the set of points spread out in a line at around $E_i \sim -7$ eV and grouped around structure plot lines 8 and 9 and the extreme ends of 11, 12, 15, and 17. It is clear that this grouping of points must come from the lowest part of band 2, near X on the Σ line, since no other states are so deep. Accordingly, we are justified in assigning $\mathbf{k}_\perp$ from the close-lying structure plot lines and mapping these points back onto the band-structure plots. The points lie among the rather dense grouping of points following the same final bands on the right-hand part of the band-structure diagram.

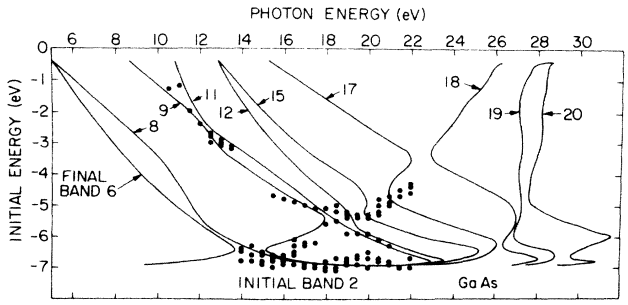

FIG. 9. Theoretical (solid lines) and experimental (closed circles) structure plot for GaAs from initial band 2 to final bands 6—20. Odd-parity final bands are omitted.

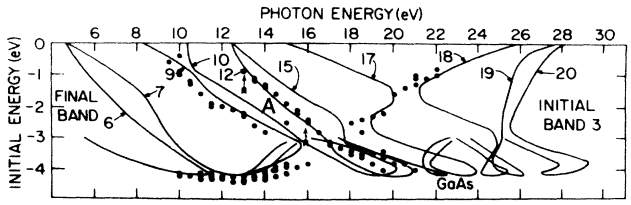

FIG. 10. Theoretical (solid lines) and experimental (closed circles) structure plot for GaAs from initial band 3 to final bands 6—20. Odd-parity final bands are omitted.

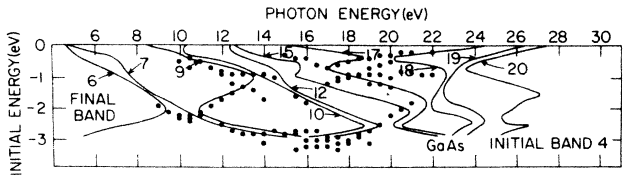

FIG. 11. Theoretical (solid lines) and experimental (closed circles) structure plot for GaAs from initial band 4 to final bands 6—20. Odd-parity final bands are omitted.

The peaks in original data corresponding to these points can be found in Figs. 12, 13, and 14, where the initial and final bands are identified for each peak. Considering now another example, the evolution with photon energy of the peaks between the arrows and denoted *A* in the EDC's of Fig. 12, we see from the structure plot, Fig. 10, that the string of corresponding points between the arrows denoted *A* coincide closely with the theoretical structure plot for bands 3 and 12.

Although some residual ambiguities remain, it is possible to determine the origin of most of the features in the spectra. In particular, the initial energies corresponding to the critical points X_3, X_5, and $\Sigma_{\min}$ were determined and, as discussed below, the theoretical bands were adjusted accordingly by a linear interpolation between the adjusted critical points. The resulting bands are the ones that are displayed here.

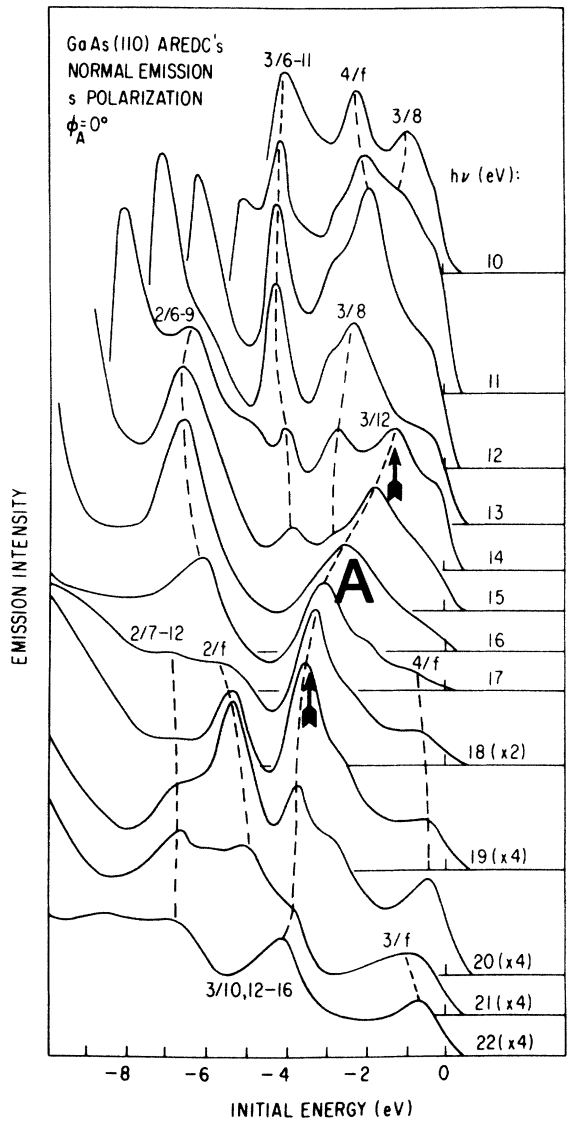

FIG. 12. Photoemitted angle-resolved energy distribution curves obtained from the GaAs(110) surface. The numbers correspond to the assignments of the pair of bands involved in the particular transition. Transitions marked *A* can be seen on the structure plot of Fig. 13.

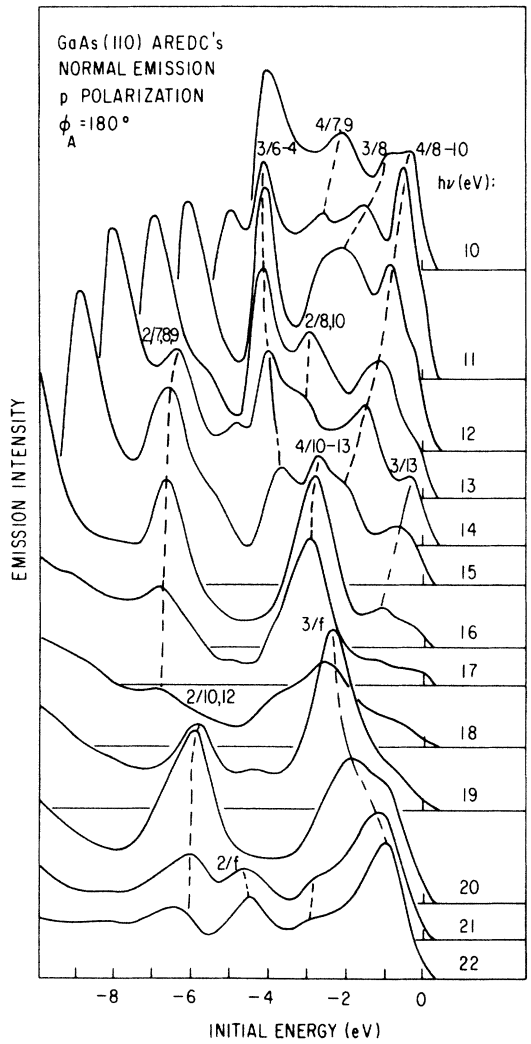

FIG. 13. Photoemitted angle-resolved energy distribution curves obtained from the GaAs(110) surface. The numbers correspond to the assignments of the pairs of bands involved in the particular transition.

TABLE II. Critical point energies (data for InSb for guidance only).

	X_5		Σ_1^{min}		X_3	
	Ref. 1	This work	Ref. 1	This work	Ref. 1	This work
GaP	2.73	2.9	4.2	4.4	7.07	6.8
GaAs	2.9	2.8	4.2	4.2	6.9	6.9
GaSb	2.5	2.4	3.6	3.7	6.76	6.3
InP	2.08	2.2	3.3	3.7	6.01	6.0
InAs	2.42	2.7	3.4	3.5	6.64	6.0
InSb	2.34	(2.3)	3.4	(3.3)	6.43	(6.7)

IV. DISCUSSION

The theoretical and experimental energy bands in Figs. 15, 16, and 17 are in generally good agreement over a wide range of energies. Note that "theoretical" lines do not represent the results of a single calculation. In general, we found better correspondence with the calculations of Pandey[2] for the final bands and with Chelikowsky and Cohen[1] for the initial bands. These raw calculations, both based on nonlocal pseudopotentials which are chosen to fit optical critical-point energies and valence-band widths, properly predicted the ordering of the bands and their general shapes. The so-called "theoretical bands" in Figs. 15, 16, and 17 have been further modified by us, either by a rigid shift of the valence bands relative to the conduction bands, or by relative stretchings and contractions at bands 2, 3, and 4 between their intercepts on the Γ and X

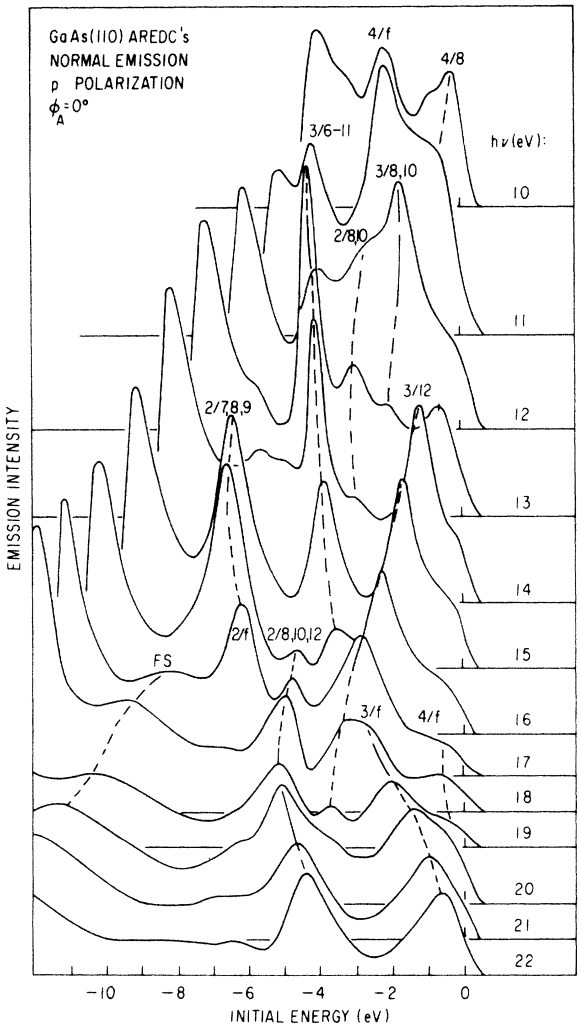

FIG. 14. Photoemitted angle-resolved energy distribution curves obtained from the GaAs(110) surface. The numbers correspond to the assignments of the pair of bands involved in the particular transition.

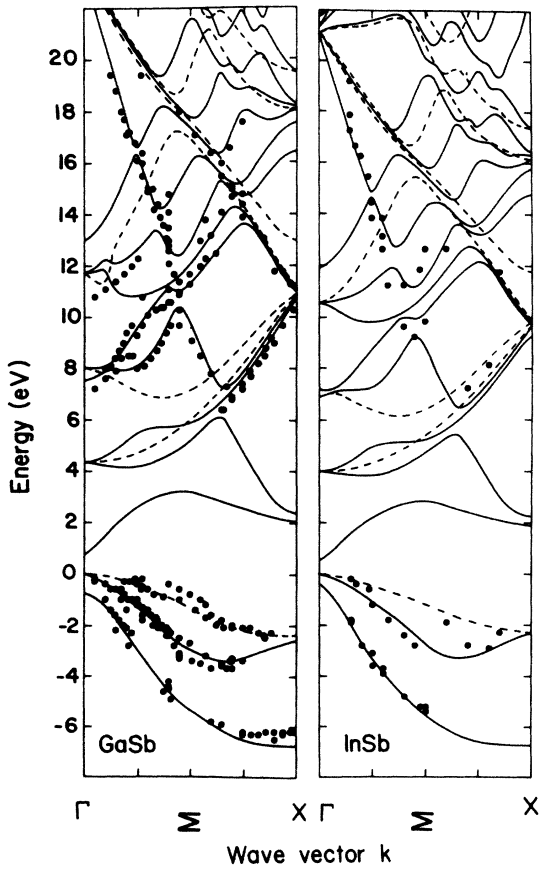

FIG. 15. Band-structure plots in the direction for GaSb and InSb. The closed circles represent the experimental results and the solid and dashed lines are the modified theoretical band structure for even or odd bands, respectively, obtained as described in the text.

axes. Some small discrepancies can still be observed, such as the X_3 level in GaP and the X_5 level in InAs. The data for GaSb and particularly InSb are insufficient to draw conclusions as definitive as those for the other materials. The critical-point energies determined from our analysis are given in Table II where they are compared with the calculations of Chelikowsky and Cohen.[1] Experimental points for GaAs, InAs, and GaP cover virtually the entire Σ line for bands 2, 3, and 4 and lie, in almost all cases, quite close to our modified theoretical valence bands. A reasonable correspondence between theory and experiment also occurs for the other materials.

A large share of the observed transitions end on the portion of the free-electron parabola sloping steeply upwards to the left in the band diagram. Along this parabola the dominant plane wave in the Fourier expansion of the wave function points along the surface normal, towards the detector. Gaps occur where this band hybridizes with other even free-electron bands, whose wave vectors are carried away from the detector direction. Final states with significant (110) plane-wave amplitude exist in these gaps, namely the states account for the experimental points within gaps of the band structure in Figs. 15, 16, and 17.

Since all even bands may hybridize with the (110) free-electron band, many of the transitions we observed end on segments of the free-electron parabola which cross the (110) band. The hybridization or "umklapp" may be attributed to surface as well as bulk potential scattering. Final bands lowest in energy—but above the vacuum level—are most prominent because the unklapp momenta are smallest. As observed in materials such as Al and Be (Refs. 12 and 13), umklapp effects are most effective near crossovers with the dominant free-electron band.

Although the transitions observed in all materials appeared to obey the selection rule[14] (i) that the final state have even reflection parity in the mirror plane, we often observed transitions from initial bands which violated rule (ii) that even bands (2 and 3) are excited only when **A** has a component lying in the MP, while for band 4 (odd) excitation requires a component of **A** perpendicular to the MP. Several effects could cause a breakdown of the symmetry upon which the selection rules are based. Spin-orbit coupling hybridizes even and odd states, and would have the largest effect on initial states with substantial *s* character. The more extended final states would be less affected by spin-orbit coupling. Our data, all of which can be understood without using odd final bands, are con-

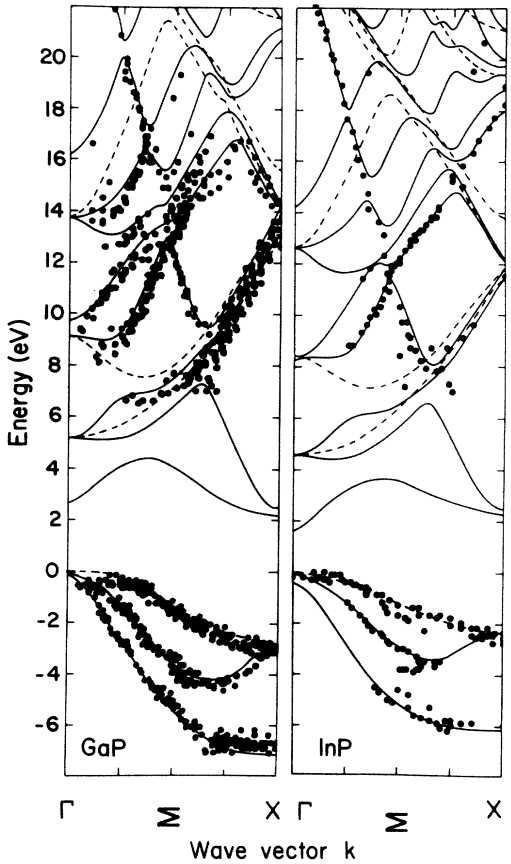

FIG. 16. Band-structure plots in the direction for GaP and InP. The closed circles represent the experimental results and the solid and dashed lines are the modified theoretical band structure for even or odd bands, respectively, obtained as described in the text.

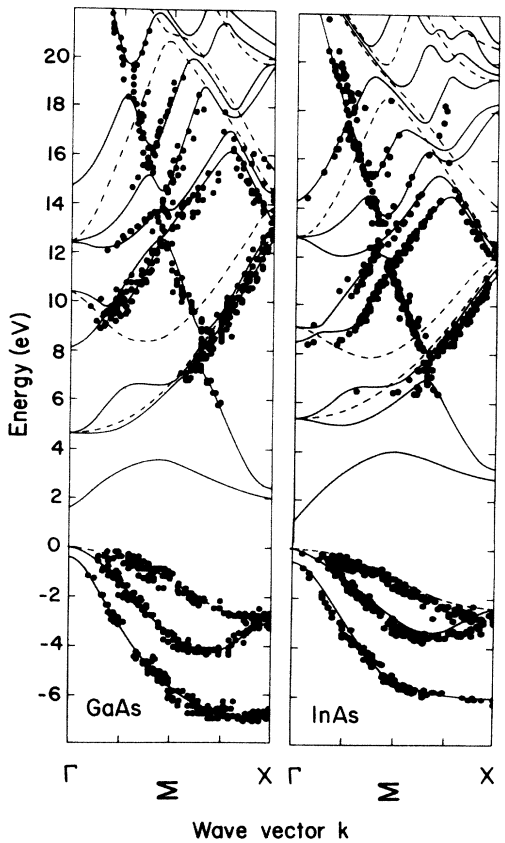

FIG. 17. Band-structure plots in the direction for GaAs and InAs. The closed circles represent the experimental results and the solid and dashed lines are the modified theoretical band structure for even or odd bands, respectively, obtained as described in the text.

sistent with this mechanism. Spin-orbit mixing should increase from P to Sb compounds and be most prominent in bands 2 and 3. These trends cannot be confirmed in our data, however, reflection symmetry could also be broken by local disorder, whether at the surface or in the bulk. Local disorder might also have a stronger influence on initial states. Finally, imperfect polarization of the incidence light mixes initial-state symmetries while retaining the selection rule requiring even final states.

In summary, we have used a technique for band mapping which is applicable even for cases of large densities of energy bands such as those found in the III-V compounds. The technique relies on an approximate calculation at the band structure in order to associate photoemission peaks with definite band pairs and wave vectors, but uses the measured peak positions to fine tune the band energies. We have exploited polarization selection rules to simplify the spectra and their interpretation. Our analysis did not require the use of final-state bands having odd reflection parity, however, numerous transitions appear to involve initial states which do not transform like the dipole operator as required by the selection rules derived for an ideal surface. Spin-orbit coupling, structural disorder, or impure polarization may explain the discrepancies we observed. Our method may be useful for band mapping in other materials with complex final bands. A more complete analysis of the method and its applications will be found in Ref. 15.

ACKNOWLEDGMENTS

We are extremely grateful to K. Pandey for communicating details of his calculation and for helpful comments. The staff at the Synchrotron Radiation center, Stoughton, of the University of Wisconsin—Madison, especially R. Otte and E. Rowe, were extremely supportive and vital to the success of these experiments, as were our colleagues P. Gobby and J. Knapp. The Synchrotron Radiation Center was supported by the National Science Foundation under Grant No. DMR-74-15089. The work was supported by the U.S. Air Force Office of Scientific Research under Contract No. F49620-77-C-0125 and in part by the U.S. Department of Energy under Contract No. DE-AC02-76CH00016. This research was also supported by the Office of Basic Energy Sciences, U.S. Department of Energy.

[1]J. R. Chelikowsky and M. L. Cohen, Phys. Rev. B **14**, 556 (1976).

[2]K. Pandey (private communication).

[3]T.-C. Chiang, J. A. Knapp, M. Aono, and D. E. Eastman, Phys. Rev. B **21**, 3513 (1979).

[4]R. Pinchaux, F. Houzay, and G. M. Guichar, Proceedings of the 6th International Conference on Vacuum Ultraviolet Spectroscopy, Charlottesville, Virginia, p. I-6 (unpublished).

[5]K. A. Mills, D. Denley, P. Perfetti, and D. Shirley, Solid State Commun. **30**, 743 (1979).

[6]L. Ley and M. Cardona, in *Topics in Applied Physics*, edited by L. Ley and M. Cardona (Springer, Berlin, 1979), Vol. 27, pp. 11—172.

[7]G. P. Williams, F. Cerrina, J. Anderson, G. J. Lapeyre, R. J. Smith, J. Hermanson, and J. A. Knapp, Physica (Utrecht) **117&118B**, 350 (1982).

[8]J. A. Knapp, G. J. Lapeyre, N. V. Smith, and M. M. Tramm, Rev. Sci. Instrum. **53**, 781 (1982).

[9]G. J. Lapeyre, R. J. Smith, and J. Anderson, J. Vac. Sci. Technol. **14**, 384 (1977).

[10]M. I. Cohen and T. K. Bergstresser, Phys. Rev. **141**, 789 (1966).

[11]See AIP document No. PAPS-PRBMD-34-5548-40 for 40 pages of tabulated theoretical structure plots. Order by PAPS number and journal reference from American Institute of Physics, Physics Auxiliary Publication Service, 335 East 45th Street, New York, N.Y. 10017. The prepaid price is $1.50 for each microfiche (98 pages) or $5.00 for photocopies of up to 30 pages, and $0.15 for each additional page over 30 pages. Airmail additional.

[12]H. J. Levinson, F. Greuter, and E. W. Plummer, Phys. Rev. B **27**, 727 (1983).

[13]E. Jensen, R. A. Bartinski, T. Gustafsson, E. W. Plummer, G. Hoflund, M. Y. Chou, and M. L. Cohen (unpublished).

[14]J. Hermanson, Solid State Commun. **22**, 9 (1977).

[15]F. Cerrina (unpublished).